Journal of
Applied
Crystallography
ISSN 1600-5767

Received 23 April 2014
Accepted 22 December 2014

Neutron Laue diffraction study of the complex low-temperature magnetic behaviour of brownmillerite-type $Ca_2Fe_2O_5$

Josie E. Auckett,[a]* Garry J. McIntyre,[b] Maxim Avdeev,[b] Hank De Bruyn,[a] Thiam Teck Tan,[c] Sean Li[c] and Chris D. Ling[a]

[a]School of Chemistry, The University of Sydney, Sydney, NSW 2006, Australia, [b]The Bragg Institute, Australian Nuclear Science and Technology Organisation, New Illawarra Road, Lucas Heights, NSW 2234, Australia, and [c]School of Materials Science and Engineering, The University of New South Wales, NSW 2052, Australia. Correspondence e-mail: josie.auckett@sydney.edu.au

The atomic and magnetic structure of brownmillerite $Ca_2Fe_2O_5$ has been refined against single-crystal neutron Laue diffraction data collected at 300, 100 and 10 K under zero-field and low-magnetic field (35 Oe = 35 × $10^3/4\pi$ A m^{-1}) conditions. $Ca_2Fe_2O_5$ is a canted G-type antiferromagnet with $Pcm'n'$ symmetry, the magnetic moments on Fe being directed approximately along the crystallographic c axis at room temperature. The refinement results show clearly that this magnetic structure persists down to T = 10 K, despite a previous suggestion that an anomalous magnetic susceptibility enhancement observed in $Ca_2Fe_2O_5$ single crystals between 40 and 140 K might signify a reorientation of the antiferromagnetic easy axis from c to a below 40 K. Alternative explanations for this susceptibility anomaly are considered in terms of the evidence for partial or short-range loss of order in the anomalous regime, possibly due to the presence of multiple competing sublattice interactions.

1. Introduction

The family of perovskite-derived brownmillerites $A_2B_2O_5$ (A = alkali earth or La; B = Al, Ga or first-row transition metal) has been the subject of numerous studies focused on their structural, dynamical, magnetic and catalytic properties. While the majority of research efforts have been directed towards ionic conductive brownmillerites having potential application as oxygen-conducting membranes in solid-oxide fuel cells, such as $Ba_2In_2O_5$ (Berastegui *et al.*, 2002) and $Sr_2Fe_2O_5$ (Leonidov *et al.*, 2006), a considerable number of brownmillerites with poorer conductivity have also been recently investigated because they exhibit interesting crystallographic or magnetic behaviours.

Almost all magnetically ordered brownmillerites adopt the G-type antiferromagnetic (AFM) structure, with unpaired spins on the B cations counter-aligned along one of the primary axes of the orthorhombic unit cell. A small number of AFM brownmillerites are also known to display weak ferromagnetic (FM) canting perpendicular to the AFM spin orientation. One such material is $Ca_2Fe_2O_5$ (Fig. 1), which has attracted recent attention following the discovery by Maljuk *et al.* (2003) of an unexplained magnetic susceptibility anomaly between T_1 = 60 K and T_2 = 140 K. Susceptibility measurements performed on oriented single crystals of $Ca_2Fe_2O_5$ were later used by Zhou & Goodenough (2005*a*) to propose that the origin of this anomaly was a reorientation of the AFM easy axis from the **c** direction to the **a** direction below T_1. The enhanced susceptibility observed in the interval $T_1 < T < T_2$ was then attributed to an intermediate regime between the two AFM phases, in which reduced magnetocrystalline anisotropy allowed the spins to be easily reoriented by a small applied field.

Despite the wealth of information that neutron scattering provides about magnetic ordering in solids, the low-temperature magnetic structure of $Ca_2Fe_2O_5$ has never been directly refined against diffraction data. Berastegui *et al.* (1999) refined the room-temperature structure in the Shubnikov space group $Pcm'n'$ against neutron powder diffraction (NPD) data, but only allowed the dominant z component (M_z) of the Fe magnetic moments to refine, yielding a purely AFM result as dictated by the Fe site symmetries. More recently, Ceretti *et al.* (2012) refined the same structure against neutron diffraction data obtained from high-quality single crystals, but also applied the $M_x = M_y = 0$ constraint to both Fe sites and did not report any refinements at non-ambient temperatures, even though the intensities of several magnetic and nonmagnetic reflections were compared between 3 and 700 K. Magnetic susceptibility measurements have long established the presence of significant FM canting in $Ca_2Fe_2O_5$, so the results of these refinements can only be said to represent a first approximation to the true magnetic structure of the material at room temperature.

The ability to refine meaningfully the FM canting in the $Ca_2Fe_2O_5$ structure is highly dependent on the quality of the neutron diffraction data, because the magnetic component of

the total neutron scattering is relatively small and is dominated by the signal from the ordered moments in AFM alignment [around one order of magnitude greater than the components in the FM alignment (Marchukov *et al.*, 1993; Takeda *et al.*, 1968)]. In practice, the loss of information due to spherical averaging in NPD data renders diffraction from powder samples unsuitable for determining such subtle effects by structure refinement alone, even with modern diffractometers. Fortunately, a number of experimental studies in the past 20 years have demonstrated the reliability of floating-zone (FZ) growth methods for obtaining large high-quality single crystals of $Ca_2Fe_2O_5$ for use in magnetization and magnetic susceptibility (Maljuk *et al.*, 2003; Marchukov *et al.*, 1993; Zhou & Goodenough, 2005*b*), Fourier spectroscopy (Brotzeller *et al.*, 1992), and dilatometry (Labii *et al.*, 2013) experiments. However, detailed crystallographic studies have not yet been reported for such crystals below room temperature. Here, we present the first full refinements of the canted magnetic structure of $Ca_2Fe_2O_5$ against single-crystal neutron diffraction data collected at room temperature, as well as between and below the two reported phase transitions T_1 and T_2. For a true comparison of the experimental conditions with those of the magnetic susceptibility experiments in which the anomaly was first observed, we have also repeated these structure refinements against diffraction data collected from a crystal in a small applied magnetic field. The bearing of these results on the interpretation of the observed susceptibility anomaly is then discussed.

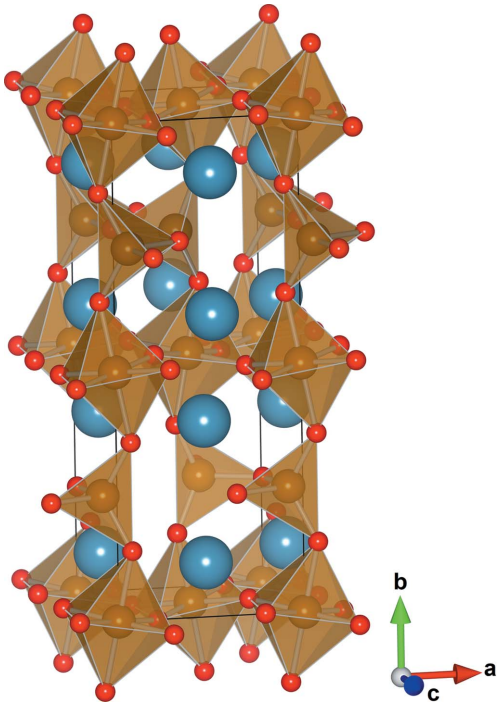

Figure 1
The brownmillerite structure of $Ca_2Fe_2O_5$ with *Pcmn* symmetry (large blue spheres: Ca; brown spheres: Fe; red spheres: O).

2. Experimental procedures

2.1. Powder synthesis

Polycrystalline $Ca_2Fe_2O_5$ samples were prepared from an intimate mixture of $CaCO_3$ (Merck, 99%) and Fe_2O_3 (Aithaca, 99.999%). Both reagents were dried overnight at 673 K before use. Stoichiometric quantities were blended in an ethanol slurry and milled for 30 min in a planetary ball mill using agate media. The air-dried powders were then annealed repeatedly at 1273–1473 K for 48 h in air, with intermediate regrinding between steps, until pure $Ca_2Fe_2O_5$ powder was obtained. Impurities formed during the early stages of the synthetic procedure (*e.g.* CaO and $CaFe_2O_4$) typically fell below the detection threshold of laboratory X-ray diffraction (XRD) after four to five annealing cycles. XRD data were collected in the range $10 \leq 2\theta \leq 70^\circ$ using a PANalytical X'Pert Pro MPD diffractometer operating in Bragg–Brentano geometry and using Cu $K\alpha$ radiation with an Ni filter.

2.2. Floating-zone crystal growth

To prepare feed rods suitable for FZ growth, $Ca_2Fe_2O_5$ powder (around 20 g) was loaded into soft rubber tubes, evacuated and pressed at 40 MPa in a hydrostatic press. The sample rods thus obtained were sintered at 1473 K for 12 h in air or flowing oxygen. The relatively low density of $Ca_2Fe_2O_5$ tended to cause poor packing of the powder inside the rubber tubes, so that the sintered rods were semi-porous and produced bubbles in the molten zone during crystal growth. A second sintering step, performed at 1523 K for 24 h with the rod suspended vertically and rotating at 10 r min^{-1}, considerably improved the packed density of the feed rods, so that only a few bubbles were observed during subsequent growths.

The single crystal of $Ca_2Fe_2O_5$ was grown in a Crystal Systems Corporation optical FZ furnace equipped with 4 × 300 W halogen lamps. A pure oxygen environment was maintained at 1.7–2.0 atm (1 atm = 101 325 Pa), in accordance with previously published procedures (Maljuk *et al.*, 2003). The growth rate was 1.00 mm h^{-1} with counter rotation of the feed and seed rods at 25 r min^{-1}.

2.3. Physical property measurements

Magnetization and magnetic susceptibility were measured using the P525 Vibrating Sample Magnetometer option of a Quantum Design Physical Property Measurement System (PPMS). Magnetic susceptibility data were collected in the range $2 \leq T \leq 300$ K on an oriented bar cut from the FZ-grown crystal, with the crystallographic *b* axis (stacking axis) arranged perpendicular to the applied field. A very weak field of only 200 Oe (1 Oe = $10^3/4\pi$ A m^{-1}) was used to reveal the expected anomaly between T_1 and T_2, which is overpowered by higher fields (Zhou & Goodenough, 2005*b*). The sample was packed into a polymer capsule with beeswax to prevent movement of the crystal during data collection. Magnetization data were collected on the same sample at 300 and 2 K in the range $-5 \leq H \leq 5$ kOe at a continuous sweep rate of 20 Oe s^{-1}.

Heat capacity measurements were performed using the relaxation technique implemented in the PPMS Heat Capacity option. Data were collected on a piece of the FZ-grown crystal in the range 10–200 K at 1 K intervals, with a total dwell time of 5 min per step.

2.4. Neutron powder diffraction

NPD data (λ = 2.4395 Å) were collected on a freshly prepared polycrystalline sample of $Ca_2Fe_2O_5$ from T = 300 K to T = 3 K at 25 K intervals. Data were collected in the range $5 \leq 2\theta \leq 165^\circ$ using the high-resolution diffractometer ECHIDNA (Liss *et al.*, 2006) at the OPAL research reactor, ANSTO, Australia. Samples were loaded into vanadium cans and cooled in an He cryofurnace.

2.5. Single-crystal neutron Laue diffraction

Variable-temperature single-crystal neutron Laue diffraction data, with and without an applied magnetic field, were collected using the Laue diffractometer KOALA (Edwards, 2011) at OPAL. A high-quality crystal fragment approximately 1 mm^3 in volume was selected for the collection of comprehensive data sets at 10, 100 and 300 K. During the zero-field experiment, the sample was attached to a simple aluminium mounting pin using fluorinated grease and enclosed inside an He cryofurnace. Each data set consisted of 13 successive Laue patterns separated by 17° rotation intervals of the instrumental φ axis (perpendicular to the incident beam), each of which was collected for 55 min. For data collection in a magnetic field, a bespoke aluminium sample mount was designed, incorporating two permanent rare-earth magnets (3 × 10 mm diameter) positioned above and below the sample at a separation of ∼70 mm, providing a field of approximately 35 Oe measured at the sample (Fig. 2). The slightly plate-shaped crystal was positioned so that the field direction was perpendicular to the largest face, which did not appear to correspond to any major crystallographic axis. The appearance of the 010 reflection on several Laue patterns confirmed that the b axis was not parallel to the field. Obstruction of the incident neutron beam by the sample mount limited the achievable φ-rotation coverage, so the 13 patterns collected for each in-field diffraction data set were separated by only 9° steps in φ. At the conclusion of the experiment the crystal was rotated on its pin by hand, maintaining the same approximate vertical orientation, and a further 13 patterns were collected at each temperature point. Additional in-field diffraction data sets consisting of 13 × 30 min patterns at 15° φ intervals were collected on VIVALDI (McIntyre *et al.*, 2006) at the Institut Laue–Langevin, Grenoble, France, using the same instrumental setup and sample mounting system.

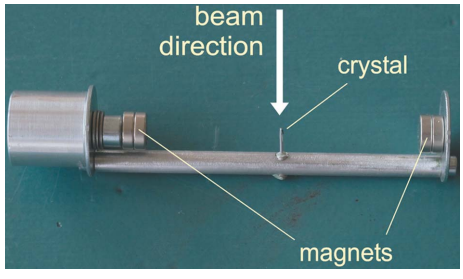

Figure 2
Sample mount used during in-field neutron Laue diffraction experiments on VIVALDI and KOALA.

The Laue patterns were indexed to a primitive orthorhombic cell with no symmetry elements imposed using the program *LAUEGEN* of the Daresbury Laboratory Laue Suite (Campbell, 1995; Campbell *et al.*, 1998) and the reflections integrated using the program *INTEGRATE+*, which uses a two-dimensional version of the minimum $\sigma(I)/I$ algorithm (Wilkinson *et al.*, 1988). The reflections within each data set were normalized to a common incident wavelength, using a curve derived by comparing equivalent reflections and multiple observations, and corrected for the different angles of incidence *via* the local program *LAUE4* (Piltz, 2011). Reflections were observed with wavelengths between 0.8 and 5.2 Å, but only those with wavelengths between 0.85 and 1.7 Å were accepted for scaling, as those outside this range were too weak or had too few equivalents to be able to determine the normalization curve with confidence. Reflections having $I < 2\sigma(I)$ were excluded from structure refinements.

2.6. Structure refinements

Combined atomic and magnetic structure refinements against both single-crystal and powder neutron diffraction data were carried out in *Jana2006* (Petříček *et al.*, 2014) using the standard magnetic form factor for Fe^{3+}. All components of the magnetic moments on both Fe sites were allowed to refine freely within the symmetry constraints of the magnetic space group. Other refined parameters included fractional coordinates and anisotropic displacement parameters for each atomic site, an extinction parameter G_{iso} (Type 1 isotropic Gaussian extinction model), and one scale factor. For NPD data, the unit-cell dimensions, zero shift, background function (Chebyschev polynomial with five terms) and peak shape (pseudo-Voigt function with parameters G_U, G_V, G_W, L_X, L_Y and the Simpson asymmetry parameter asym) were also refined. Two constrained isotropic displacement parameters were shared by the three metal sites and the three oxygen sites, respectively. Bond valence sum (BVS) calculations (Brese & O'Keeffe, 1991) were performed in *Jana2006* with a fixed d_{max} cutoff of 3.5 Å.

3. Results

3.1. Magnetic measurements

Data collected on a piece of the FZ-grown single crystal of $Ca_2Fe_2O_5$ with the field applied perpendicular to **b** showed the expected enhancement of the magnetic susceptibility in a well defined interval, $T_1 < T < T_2$, below room temperature (Fig. 3). Zhou and Goodenough have noted that the transition temperature T_1 is sample dependent; our measured value of T_1 = 55 K lies between the literature values of 40 K (Zhou &

Table 1
Structural parameters of $Ca_2Fe_2O_5$ refined against NPD data.

For the 300 K data: $R_p = 0.0166$, $wR_p = 0.0229$, GOF = 1.61 for 36 parameters; $a = 5.42507$ (11), $b = 14.7746$ (3), $c = 5.59295$ (11) Å. For the 25 K data: $R_p = 0.0149$, $wR_p = 0.0200$, GOF = 1.64 for 36 parameters; $a = 5.42194$ (13), $b = 14.7317$ (3), $c = 5.58759$ (13) Å.

	x (a)	y (b)	z (c)	$100U_{iso}$ (Å^2)†	m_x (μ_B/Fe)	m_y (μ_B/Fe)	m_z (μ_B/Fe)
300 K							
Ca1	0.9776 (4)	0.10758 (12)	0.4801 (5)	0.46 (5)	–	–	–
Fe1	0	0	0	0.46 (5)	−0.87 (13)	0.13 (7)	4.03 (4)
Fe2	0.0649 (3)	0.25	0.9466 (3)	0.46 (5)	−0.53 (11)	–	−3.63 (4)
O1	0.7647 (5)	0.98382 (13)	0.2630 (6)	0.58 (5)	–	–	–
O2	0.9282 (3)	0.14059 (13)	0.0250 (4)	0.58 (5)	–	–	–
O3	0.1267 (6)	0.25	0.5975 (5)	0.58 (5)	–	–	–
25 K							
Ca1	0.9785 (4)	0.10775 (13)	0.4774 (5)	0.25 (5)	–	–	–
Fe1	0	0	0	0.25 (5)	−0.63 (15)	0.12 (7)	4.27 (4)
Fe2	0.0645 (3)	0.25	0.9477 (3)	0.25(5)	−0.33 (14)	–	−3.97 (4)
O1	0.7667 (4)	0.98351 (13)	0.2685 (5)	0.31 (5)	–	–	–
O2	0.9260 (3)	0.14015 (13)	0.0269 (4)	0.31 (5)	–	–	–
O3	0.1260 (6)	0.25	0.5971 (5)	0.31 (5)	–	–	–

† Shared isotropic displacement parameters were defined for (Ca1, Fe1, Fe2) and (O1, O2, O3).

Goodenough, 2005*b*) and 60 K (Maljuk *et al.*, 2003). Our observation of $T_2 = 140$ K is also in agreement with these previous studies.

The magnetization curve measured at 300 K reveals a narrow hysteresis loop with a positive slope, consistent with the presence of weak ferromagnetism in $Ca_2Fe_2O_5$. The step-like appearance of the curve can be attributed to the reorientation of individual magnetic domains in the crystal; the clear reproducibility of these steps and their approximate symmetry about the loop centre suggest that these domains are well defined by a small number of fixed defects in the crystal.

3.2. Heat capacity

Heat capacity data collected for a fragment of the same crystal show the smooth behaviour expected for an oxide at low temperatures, with no evidence for any long-range ordering transitions in the measured temperature range (Fig. 4).

3.3. Neutron powder diffraction

As found by Berastegui *et al.* (1999), refinements of the combined atomic and magnetic structure of $Ca_2Fe_2O_5$ against NPD data satisfactorily reproduced the expected G-type AFM structure in $Pcm'n'$ with spins approximately parallel to **c**. In addition, the refined M_x parameters for both Fe sites suggested weak FM canting in the **a** direction (Table 1). The NPD data also offer the advantage of unambiguously revealing the diagnostic pair of magnetic reflections 021/120, which do not appear in every single-crystal Laue diffraction data set because of the incomplete Q coverage of those experiments. A reorientation of the AFM easy axis from the c axis to the a axis should be accompanied by an inversion of the

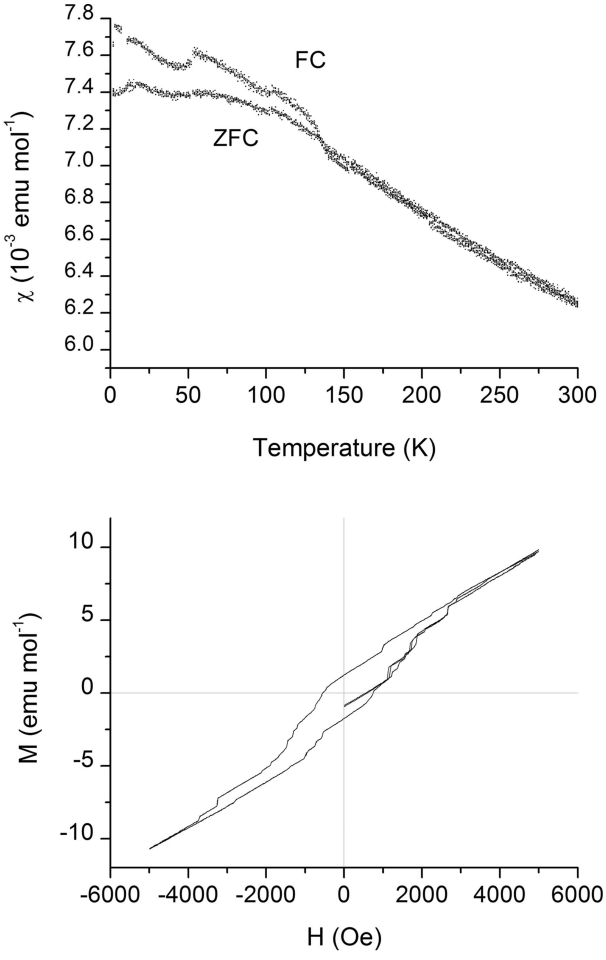

Figure 3
(*a*) Magnetic susceptibility data from a $Ca_2Fe_2O_5$ single crystal, collected using a field of 200 Oe applied perpendicular to the crystallographic b axis. (*b*) Magnetization curves (two cycles shown) collected on the same crystal at 300 K.

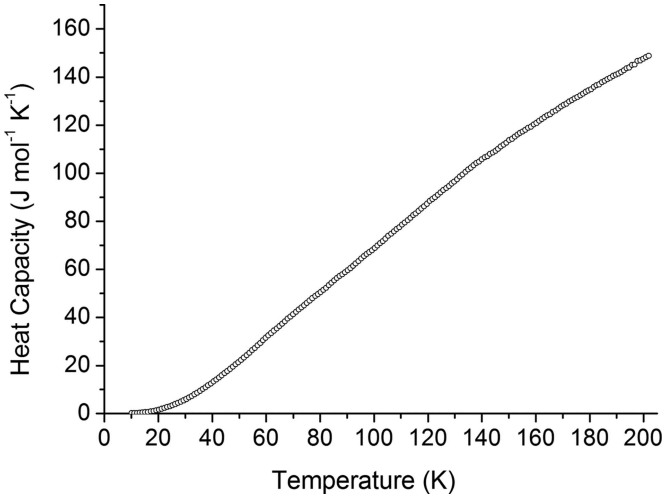

Figure 4
Heat capacity data for single-crystalline $Ca_2Fe_2O_5$. Error bars are smaller than the symbols.

Table 2
The canted magnetic structure of $Ca_2Fe_2O_5$ refined against single-crystal neutron Laue diffraction data at 300 K.

R = 0.0608, wR = 0.0512, GOF = 1.70 for 8738 reflections (55 parameters).

	x (a)	y (b)	z (c)	Fractional occupancy	$100U_{iso}$ (Å^2)	BVS	m_x (μ_B/Fe)	m_y (μ_B/Fe)	m_z (μ_B/Fe)
Ca1	0.97706 (8)	0.10790 (5)	0.48088 (9)	1	0.794 (15)	1.936 (3)	–	–	–
Fe1	0	0	0	1	0.539 (10)	3.022 (3)	−1.17 (4)	0.100 (11)	4.143 (14)
Fe2	0.06612 (5)	0.25	0.94597 (6)	1	0.459 (9)	2.921 (2)	−0.68 (4)	–	−3.663 (13)
O1	0.76322 (17)	0.9839 (2)	0.26299 (16)	0.991 (14)	0.72 (2)	2.051 (3)	–	–	–
O2	0.92741 (8)	0.14069 (3)	0.02386 (7)	1.005 (3)	0.953 (13)	1.8529 (15)	–	–	–
O3	0.12579 (9)	0.25	0.59786 (10)	0.996 (4)	0.690 (16)	2.0330 (19)	–	–	–

intensity ratio of these two reflections from approximately 1/3 to 3 (Friedman *et al.*, 1967), but we observed no significant variation in the relative intensities of these two reflections between 300 and 3 K (Fig. 5), in agreement with previous reports (Ceretti *et al.*, 2012).

3.4. Zero-field neutron Laue diffraction

The refinement against single-crystal Laue diffraction data at 300 K[1] yielded far more precise results than the NPD refinements of §3.3, reproducing both the AFM structure and significant FM canting with a high degree of certainty. The quality of the data was such that anisotropic displacement parameters could be refined reliably for all atomic sites, while the refined fractional occupancies of the three O sites were very close to the expected stoichiometry (Table 2). The total spin moment calculated from the M_x and M_z components at the octahedral Fe site was 4.31 (1) μ_B, in good agreement with the literature (Takeda *et al.*, 1968). The value of 3.73 (1) μ_B at the tetrahedral site was slightly lower, consistent with the fewer $M-O-M$ exchange pathways available from this site compared to the octahedral site. The magnitude of the FM moment in the **a** direction was 0.93 (4) μ_B/Fe.

The refinement at 10 K was attempted in both the room-temperature ($Pcm'n'$) and the predicted low-temperature ($Pcm'n'$) magnetic space groups. Given the locations of the two unique Fe atoms at 4*a* and 4*c* Wyckoff sites in the brownmillerite unit cell, the time-reversal symmetries in $Pcm'n'$ and $Pc'm'n$ allow a nonzero net moment in only the **a** and **c** directions, respectively (Table 3). The chosen space group therefore effectively dictates the magnetic structure that is obtained if M_x, M_y and M_z are allowed to refine freely from near-zero initial values. Although refinements using both models converged, inspection of the agreement factors [R, weighted R_w and goodness of fit (GOF)] clearly showed that the room-temperature model yielded the best fit to the 10 K data. For comparison, a test refinement of the $Pc'm'n$ model against the 300 K data set produced a similarly worse fit than the correct structure in $Pcm'n'$ (Table 4).

It is therefore clear from both the single-crystal and powder diffraction experiments that the room-temperature $Pcm'n'$ model provides the best description of $Ca_2Fe_2O_5$ at both 300

[1] Supplementary refinement data are available from the IUCr electronic archives (Reference: PD5048).

Table 3
Allowed spin components in the **a**, **b** and **c** directions for the two brownmillerite Fe sites in the magnetic space groups derived from *Pcmn*.

AF = net antiferromagnetic; F = net ferromagnetic; – = zero moment allowed in that direction.

	Fe1, octahedral (4*a*)			Fe2, tetrahedral (4*c*)		
Shubnikov group	**a**	**b**	**c**	**a**	**b**	**c**
Pcmn	AF	AF	AF	–	AF	–
$Pc'm'n'$, $Pcm'n$	–	–	–	AF	–	AF
$Pcmn'$, $Pc'mn$	–	–	–	–	AF	–
$Pc'm'n$	AF	AF	F	AF	–	F
$Pc'mn'$	AF	F	AF	–	F	–
$Pcm'n'$	F	AF	AF	F	–	AF

Table 4
Summary of magnetic structure refinements attempted for $Ca_2Fe_2O_5$ in various Shubnikov groups, including the room-temperature ($Pcm'n'$) and proposed low-temperature ($Pc'm'n$) models, against zero-field single-crystal neutron Laue diffraction data.

	10 K		100 K			300 K	
Reflections	9003		10279			8738	
	$Pcm'n'$	$Pc'm'n$	$Pcm'n'$	$Pc'm'n$	$Pc'mn'$	$Pcm'n'$	$Pc'm'n$
GOF	2.55	5.31	3.36	5.52	7.31	1.70	3.96
R	0.0601	0.0709	0.0981	0.1097	0.1201	0.0608	0.0738
R_w	0.0568	0.1185	0.0827	0.1357	0.1799	0.0512	0.1191
Parameters	55	55	55	55	54	55	55

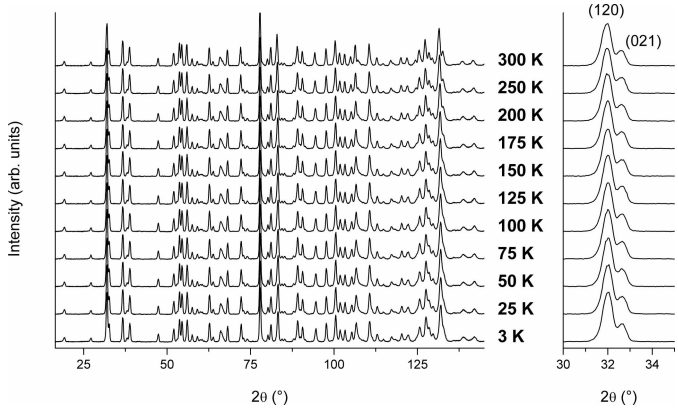

Figure 5
Neutron powder diffraction data for $Ca_2Fe_2O_5$, collected in the temperature range 3–300 K. Right: zoomed section showing the diagnostic 021/120 reflection doublet.

and 10 K; *i.e.* there is no evidence for the proposed spin reorientation below T_1.

The refinements against data collected at 100 K, in the anomalous $T_1 < T < T_2$ interval, displayed slightly different characteristics from those at 300 and 10 K. Although the compared agreement factors again favoured the room-temperature model over the reoriented model, the quality of the fit was significantly worse than at other temperatures (Table 4). A tendency for the refinement to converge at false minima was also noted. Re-initialization of the magnetic parameters with different starting values before successive refinement runs produced a series of 'converged' magnetic structures that differed slightly in the relative magnitudes and signs of M_x and M_z. After several attempts, the lowest R factors were identified for the structure corresponding most closely to the refined structures at 300 and 10 K.

Although the $Pcm'n'$ magnetic space group appears to describe the structure less well at 100 K than at the other measured temperatures, the fits provided by other ordered models are significantly worse. The absence of any additional reflections in the variable-temperature NPD data for $T_1 < T < T_2$ rules out the possibility of a magnetic superstructure in this regime, so that only the set of eight magnetic space groups based on the nuclear crystal symmetry $Pcmn$ need to be considered. Examination of Table 3 shows that only three of these ($Pc'm'n$, $Pc'mn'$, $Pcm'n'$) permit the net FM component that has been well established by previous experimental studies as well as the present one. Magnetic structure refinements were therefore attempted in both $Pc'm'n$ and $Pc'mn'$, but these did not produce satisfactory results (Table 4).

3.5. In-field neutron Laue diffraction

Although the refinement results described above can be considered conclusive, the possibility still remained that the magnetic susceptibility anomaly which led to the proposal of the spin-reoriented model was in fact stimulated by the small magnetic field used to measure it. In this case, the reorientation might not occur under the zero-field conditions of the neutron diffraction experiments. Additional single-crystal neutron Laue diffraction data were therefore collected in a magnetic field of approximately 35 Oe, within the range of fields (10–100 Oe) used by Maljuk *et al.* (2003) for their susceptibility measurements. Because the effect appears to be suppressed when the crystallographic *b* axis lies parallel to the applied field (Zhou & Goodenough, 2005*b*), care was taken to ensure that the crystal was not mounted in this orientation.

A summary of the refinements against in-field diffraction data is presented in Table 5. A small overall decrease in the magnitudes of the refined atomic displacement parameters with respect to the zero-field data was noted at 100 K. This effect may not be significant, however, because the incomplete Q coverage achieved by the Laue diffraction instrument's single axis of rotation can lead to a slightly poorer determination of displacement parameters than of atomic coordinates and scale-related factors such as site occupations. No other significant deviation from the zero-field refinement results was observed at any measured temperature. Furthermore, the integrated intensities of the 021 and 120 reflections were extracted from the reflection files generated from the KOALA raw data sets or – where one or both reflections were missing owing to incomplete angular coverage – from the VIVALDI data sets collected under comparable conditions. At all measured temperatures, the 021/120 intensity ratio was less than 1, indicating AFM spins parallel to **c** in agreement with the NPD data.

Table 5
Summary of magnetic structure refinements against single-crystal neutron Laue diffraction data collected in a 35 Oe field.

	10 K		100 K			300 K	
Reflections	9858		9145			9069	
	Pcm′n′	*Pc′m′n*	*Pcm′n′*	*Pc′m′n*	*Pc′mn′*	*Pcm′n′*	*Pc′m′n*
GOF	2.47	4.29	3.20	4.56	6.73	2.42	4.41
R	8.50	9.30	9.51	10.27	11.37	9.97	10.90
R_w	6.61	11.46	8.94	12.74	18.80	6.76	12.29
Parameters	55	55	55	55	54	55	55

4. Discussion

The magnetic susceptibility anomaly that prompted Zhou & Goodenough (2005*a*) to propose a model for spin reorientation in $Ca_2Fe_2O_5$ is certainly also present in our single-crystal samples. However, the results of all neutron diffraction experiments performed on these single crystals and on powder samples show conclusively that there is no magnetic spin reorientation below room temperature, regardless of whether an external magnetic field is present. The predominant long-range magnetic ordering in $Ca_2Fe_2O_5$ remains unchanged at all measured temperatures, including in the anomalous regime. Therefore, provided that the phenomenon is intrinsic to the material and does not arise from the presence of an impurity phase, the intermediate-temperature phase ($T_1 < T < T_2$) would appear to be distinguished only by a partial short-range loss of magnetic order. This subtle effect could give rise to the observed slight enhancement of the magnetic susceptibility, without being easily detectable in heat capacity data or quantifiable by techniques probing long-range order, such as neutron diffraction.

The reason for such a weakening of magnetic exchange in this temperature interval is unclear, but consideration of the crystal structure suggests the possibility of competing interactions between multiple magnetic sublattices. The presence of two independent magnetic ion sites (tetrahedral and octahedral) with antiferromagnetic relations implies at least two such sublattices, with a comprehensive group-theoretical analysis performed by Marchukov *et al.* (1993) suggesting as many as six. Determining the precise nature of the interactions among these sublattices lies beyond the scope of this work, but clearly they introduce a great deal of complexity to the material's local and long-range-ordered magnetic behaviour. A third transition weakly visible near T = 100 K in our susceptibility data (Fig. 3), which was also observed but not

commented upon by previous authors (Maljuk *et al.*, 2003; Zhou & Goodenough, 2005*b*), further highlights this apparent complexity.

Finally, although the possibility of a magnetic impurity phase producing the observed susceptibility anomaly cannot be positively excluded, we consider it to be improbable. Maljuk *et al.* (2003) assessed the known magnetic transition temperatures of various possible magnetic impurities in the CaO–Fe_2O_3 system and could find none corresponding closely to T_1 and T_2. In any case, the very high crystal quality established for the FZ-grown specimens used in this and other studies confirms that inclusions of impurity phases in the measured crystals are very unlikely to be present. Another possible impurity, the oxidized phase $CaFeO_3$, is an antiferromagnet with $T_N \simeq 115$ K (Woodward *et al.*, 2000). It has recently been found to display re-entrant antiferromagnetism, accompanied by anomalous enhanced susceptibility similar to that of $Ca_2Fe_2O_5$, when synthesized as nanoparticles (Ghosh *et al.*, 2013). The onset temperature of the enhancement upon cooling, however, is around 50 K higher than for $Ca_2Fe_2O_5$. In addition, the presence of $CaFeO_3$ in our single-crystal sample is implausible because of the extremely oxidizing conditions that must be applied to synthesize it directly [*e.g.* annealing $Ca_2Fe_2O_5$ at 773 K in flowing ozone (Zhou & Goodenough, 2005*a*) or at 1373 K and 20 kbar (2 GPa) in O_2 (Kanamaru *et al.*, 1970)].

5. Conclusion

Magnetic structure refinements against neutron diffraction data, collected on high-quality single-crystal and powder samples of the canted antiferromagnet $Ca_2Fe_2O_5$ under both zero-field and low-field (H = 35 Oe) conditions using a customized sample environment, show that a long-range-ordered structure at 300 K persists down to at least 10 K. There is no deviation from the magnetic space group symmetry that places the spins antiparallel along the c axis, including in the 55–140 K region where magnetic susceptibility anomalies are observed. The application of the small biasing magnetic field during diffraction data collection, in order to replicate precisely the conditions under which the magnetic susceptibility anomaly was observed, did not change the result. The magnetic anomaly is therefore attributed to competing interactions among multiple magnetic sublattices in the material, leading to subtle changes in the short-range magnetic ordering without affecting the long-range average structure.

The authors acknowledge the Australian Research Council for funding under the Discovery Projects scheme. JEA acknowledges support from the Australian Institute of Nuclear Science and Engineering under the AINSE PGRA scheme.

References

Berastegui, P., Eriksson, S. G. & Hull, S. (1999). *Mater. Res. Bull.* **34**, 303–314.
Berastegui, P., Hull, S., García-García, F. J. & Eriksson, S. G. (2002). *J. Solid State Chem.* **164**, 119–130.
Brese, N. E. & O'Keeffe, M. (1991). *Acta Cryst.* B**47**, 192–197.
Brotzeller, C., Geick, R., Marchukov, P., Rudashevsky, E. G. & Balbashov, A. M. (1992). *Solid State Commun.* **82**, 923–925.
Campbell, J. W. (1995). *J. Appl. Cryst.* **28**, 228–236.
Campbell, J. W., Hao, Q., Harding, M. M., Nguti, N. D. & Wilkinson, C. (1998). *J. Appl. Cryst.* **31**, 496–502.
Ceretti, M., Piovano, A., Cousson, A., Berthier, T., Meven, M., Agostini, G., Schefer, J., Hernandez, O., Lamberti, C. & Paulus, W. (2012). *CrystEngComm*, **14**, 5771–5776.
Edwards, A. J. (2011). *Aust. J. Chem.* **64**, 869–872.
Friedman, Z., Shaked, H. & Shtrikman, S. (1967). *Phys. Lett. A*, **25**, 9–10.
Ghosh, B., Bagani, K., Ray, M. K., Sardar, M. & Banerjee, S. (2013). *AIP Conf. Proc.* **1536**, 943–944.
Kanamaru, F., Miyamoto, H., Mimura, Y., Koizumi, M., Shimada, M., Kume, S. & Shin, S. (1970). *Mater. Res. Bull.* **5**, 257–261.
Labii, T., Ceretti, M., Boubertakh, A., Paulus, W. & Hamamda, S. (2013). *J. Therm. Anal. Calorim.* **112**, 865–870.
Leonidov, I. A., Patrakeev, M. V., Bahteeva, J. A., Poholok, K. V., Filimonov, D. S., Poeppelmeier, K. R. & Kozhevnikov, V. L. (2006). *J. Solid State Chem.* **179**, 3045–3051.
Liss, K. D., Hunter, B., Hagen, M., Noakes, T. & Kennedy, S. (2006). *Physica B*, **385–386**, 1010–1012.
Maljuk, A., Strempfer, J. & Lin, C. T. (2003). *J. Cryst. Growth*, **258**, 435–440.
Marchukov, P., Geick, R., Brotzeller, C., Treutmann, W., Rudashevsky, E. G. & Balbashov, A. M. (1993). *Phys. Rev. B*, **48**, 13538–13546.
McIntyre, G. J., Lemée-Cailleau, M. H. & Wilkinson, C. (2006). *Physica B*, **385–386**, 1055–1058.
Petříček, V., Dušek, M. & Palatinus, L. (2014). *Z. Kristallogr.* **229**, 345–352.
Piltz, R. (2011). *Acta Cryst.* A**67**, C155.
Takeda, T., Yamaguchi, Y., Tomiyoshi, S., Fukase, M., Sugimoto, M. & Watanabe, H. (1968). *J. Phys. Soc. Jpn*, **24**, 446–452.
Wilkinson, C., Khamis, H. W., Stansfield, R. F. D. & McIntyre, G. J. (1988). *J. Appl. Cryst.* **21**, 471–478.
Woodward, P. M., Cox, D. E., Moshopoulou, E., Sleight, A. W. & Morimoto, S. (2000). *Phys. Rev. B*, **62**, 844–855.
Zhou, H. D. & Goodenough, J. B. (2005*a*). *J. Solid State Chem.* **178**, 3679–3685.
Zhou, H. D. & Goodenough, J. B. (2005*b*). *Solid State Sci.* **7**, 656–659.